Laser Control of Electronic Exchange Interaction within a Molecule

Patrick Rupprecht,[1,*] Lennart Aufleger,[1] Simon Heinze,[2] Alexander Magunia,[1] Thomas Ding,[1] Marc Rebholz,[1] Stefano Amberg,[1] Nikola Mollov,[1] Felix Henrich,[1] Maurits W. Haverkort,[2] Christian Ott,[1,†] and Thomas Pfeifer[1,‡,§]

[1]*Max-Planck-Institut für Kernphysik, Saupfercheckweg 1, 69117 Heidelberg, Germany*

[2]*Institut für theoretische Physik, Ruprecht-Karls-Universität Heidelberg, Philosophenweg 19, 69120 Heidelberg, Germany*

(Received 6 October 2021; revised 1 December 2021; accepted 28 January 2022; published 11 April 2022; corrected 20 April 2022)

Electronic interactions play a fundamental role in atoms, molecular structure and reactivity. We introduce a general concept to control the effective electronic exchange interaction with intense laser fields via coupling to excited states. As an experimental proof of principle, we study the SF_6 molecule using a combination of soft x-ray and infrared (IR) laser pulses. Increasing the IR intensity increases the effective exchange energy of the core hole with the excited electron by 50%, as observed by a characteristic spin-orbit branching ratio change. This work demonstrates altering electronic interactions by targeting many-particle quantum properties.

DOI: 10.1103/PhysRevLett.128.153001

Electron-electron interaction is pivotal for molecular physics and chemistry by binding atoms together via covalent bonds. This interaction can be split into the classical direct Coulomb repulsion and the exchange interaction, which is a pure quantum effect related to the Pauli principle [1].

Light, especially when emitted by lasers, is an ideal tool to investigate [2] and control [3] molecules on this electronic level: Its tunable electric field directly couples to the charged electrons, which quickly transfer their excitation to the nuclei. This forms the basis for observing and coherently controlling molecular dynamics ranging from small diatomic [4,5] and polyatomic [6–8] up to large biologically relevant [9,10] molecules. Furthermore, in solid-state systems, macroscopic, correlation-based phenomena such as magnetism [11,12] or high-temperature superconductivity [13] can be altered via laser light.

Core-level transient absorption spectroscopy as an all-optical technique has led to scientific breakthroughs in the field of laser-induced atomic [14,15] and molecular [16–20] dynamics. To date, physical insights have been gained from experimentally quantifying parameters such as the absorption line shape [21–23], the resonance energy [24,25], and its line strength [15–17,24,25] under the influence of strong fields. High-resolution studies of static x-ray absorption spectra have identified another experimentally accessible observable: The relative area ratio of spin-orbit-split absorbance doublets. Theoretical works [26,27] have shown that a change in this so-called branching ratio [28] is a direct measure of the electronic exchange interaction. Since then, the analysis of branching ratios in x-ray absorption spectroscopy (XAS) has helped to elucidate the electronic-correlation nature even in complex solid-state systems [29].

Here, we realize laser control of the effective exchange-interaction energy. Tuning solely the electronic degrees of freedom is achieved by the ultrafast transient coupling of electronic states via intense IR laser pulses and analyzing its imprint on the spin-orbit branching ratio. Using ultrashort x-ray pulses acting on the timescale of a core-hole lifetime, the measurement is completed before significant nuclear motion sets in. To clearly single out the effect of a tuned exchange interaction, we employ an excitation from a spin-orbit-split core orbital. This serves as a proof of concept and offers element specificity within the molecule. Furthermore, our study constitutes a new mechanism for electronic structure alteration, as we do not rely on either significant population or charge transfer [30], ionization [31], nor a mediation through nuclear motion like vibrations [5], rotations [8], or intersite couplings across a lattice [11–13,32].

Our goal in this Letter is to describe and quantify exchange-interaction control using a minimal theoretical toy model (for a thorough derivation, consult Supplemental Material, Sec. III [33]). This is achieved by reducing the theoretical framework to its most important parts and introducing effective parameters [41].

In the following, we distinguish between the single- and the multiparticle perspective by referring to "orbitals" in

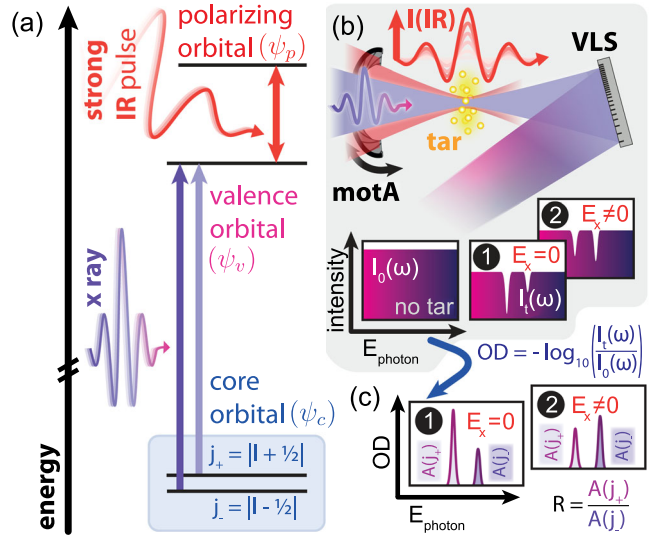

FIG. 1. Schematic experiment. (a) Single-particle-picture level scheme with spin-orbit-split core orbitals $\psi_{c_\pm}$, valence orbital ψ_v, and laser-coupled polarizing orbital ψ_p. (b) Experimental transient absorption setup scheme for exchange-interaction control (compare Supplemental Material, Sec. I [33]). A motorized aperture (motA) cuts the IR beam mode and thus controls the IR intensity. The transmitted SXR through a gaseous target (tar) is spectrally dispersed via a variable-line-spacing (VLS) grating, while the target is perturbed by the time-overlapped IR field of variable intensity. The insets show expected SXR spectra for the "no target" case and "with target" [without (1) or with (2) exchange interaction]. (c) The corresponding optical densities (ODs) of (b). In the case without exchange interaction (1), the spin-orbit peak area ratio R is given by the statistical one, derived from Pauli's principle, while deviating from it otherwise.

contrast to "states," respectively. We restrict our one-particle space to three orbitals, here denoted "core" orbital ψ_c, "valence" orbital ψ_v and "polarizing" orbital ψ_p [compare Fig. 1(a)]. A weak dipole field couples ψ_c to ψ_v, while a strong field couples ψ_v to ψ_p. The weak field will act as a "probe" in the following. Furthermore, ψ_c is assumed to experience significant spin-orbit coupling, splitting into two "core orbitals" $\psi_{c_\pm}$.

Based on the four single-particle orbitals, the many-body ground state $|0\rangle$ is created by filling the orbitals with electrons to the highest occupied molecular orbital (HOMO). In addition, the valence and the polarizing orbital of Fig. 1(a) can be dipole excited (ψ_v^1 or ψ_p^1) leaving a hole in either of the two spin-orbit-split core orbitals, $\psi_{c_\pm}^{-1}$. Thus, this gives rise to four many-body excited states: $|c_+^{-1}v^1\rangle$, $|c_-^{-1}v^1\rangle$, $|c_+^{-1}p^1\rangle$, and $|c_-^{-1}p^1\rangle$. The first two excited states $|c_\pm^{-1}v^1\rangle$ contain an electron promoted to the valence orbital from either of the two spin-orbit-split core orbitals. A further excitation of the valence electron to the polarizing orbital gives rise to the last two states $|c_\pm^{-1}p^1\rangle$. Using this many-body basis, the Hamiltonian can be expressed as the 5×5 matrix

$$H = \begin{array}{c} \begin{matrix} |0\rangle & |c_+^{-1}v^1\rangle & |c_-^{-1}v^1\rangle & |c_+^{-1}p^1\rangle & |c_-^{-1}p^1\rangle \end{matrix} \\ \begin{pmatrix} 0 & \mu_+ d\mathcal{E} & \mu_- d\mathcal{E} & 0 & 0 \\ \mu_+ d\mathcal{E} & E_+ & \boldsymbol{E_x} & d'\mathcal{E}' & 0 \\ \mu_- d\mathcal{E} & \boldsymbol{E_x} & E_- & 0 & d'\mathcal{E}' \\ 0 & d'\mathcal{E}' & 0 & E'_+ & \boldsymbol{E'_x} \\ 0 & 0 & d'\mathcal{E}' & \boldsymbol{E'_x} & E'_- \end{pmatrix} \end{array}. \quad (1)$$

The energy expectation values of $|c_\pm^{-1}v^1\rangle$ are denoted as E_+ and E_-. Their coupling to the ground state is given by the dipole matrix element d and the weak, probing field strength $\mathcal{E}$. It is weighted with a multiplicity factor $\mu_\pm \overset{\text{def}}{=} \sqrt{2j_\pm + 1}$ due to the degeneracies of $\psi_{c_\pm}$. The states are further coupled to one another by the matrix element E_x, because the electrons in the orbitals can flip their spin and position via exchange interaction. The states $|c_\pm^{-1}p^1\rangle$ give rise to an analogous block of matrix elements E'_+, E'_-, and E'_x, which are coupled to the upper-left 3×3 block by the dipole matrix element d' and the strong field $\mathcal{E}'$.

In general, the eigenvalues of the Hamiltonian matrix $H|_{\mathcal{E}=0}$ at a vanishing probe field determine the centers of the spectral line, while the areas correspond to the squares of off-diagonal matrix elements of H expressed in the diagonal basis of these eigenvectors [42]. In the absence of any field and exchange interaction, the matrix is diagonal and the spectrum of the probe field therefore shows two peaks with the expected statistical area ratio of $R = (\mu_+^2/\mu_-^2) = [(2j_+ + 1)/(2j_- + 1)]$. Because of the exchange coupling, this ratio changes [26,27], as is schematically shown in Fig. 1(c).

Additionally activating the strong field individually couples the orbitals containing the valence electron with higher-lying valence orbitals and the same core hole. This further influences the ratio, because the final states reached by the probe field now have overlap with the initially inaccessible states $|c_\pm^{-1}p^1\rangle$, which have a different exchange-interaction strength E'_x. If the excited-state lifetime is much shorter than the duration of the pulse that couples the valence to the polarizing orbital, one can evaluate H with an adiabatic approach (see Supplemental Material, Sec. V [33]) without explicit time dependence in any matrix element. This is analogous to a treatment of laser-dressed states.

For an experimental realization of electronic exchange-interaction control, the prototypical molecule sulfur hexafluoride (SF_6) was investigated using XAS in combination with strong IR laser pulses. The sulfur (S) $L_{2,3}$-edge transition to the LUMO was chosen as core-to-valence transition, visualized in Fig. 2(a). In terms of molecular orbitals (MOs), this corresponds to an electronic dipole transition from the core-level $2t_{1u}(j_\pm = \{3/2, 1/2\})$ orbital with atomic S $2p$ character ($l = 1$ and thus $j_\pm = 1 \pm 1/2$) to the $6a_{1g}$ LUMO, mediated by a soft x-ray (SXR) pulse at transition energies of 173.44 and

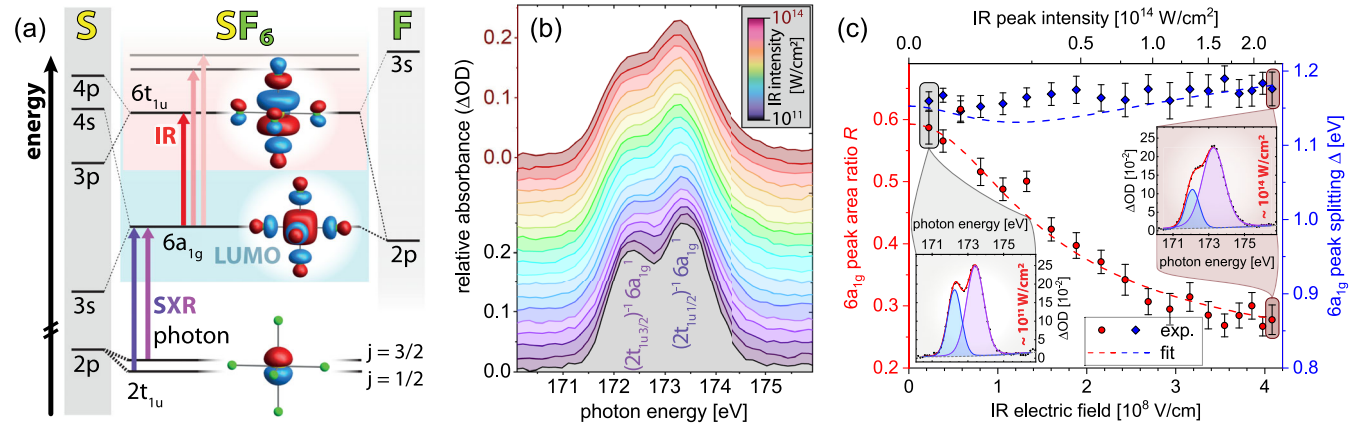

FIG. 2. SF_6 electronic structure, measured S $L_{2,3}$ absorption spectra, and derived quantities. (a) Scheme of the relevant MOs in the single-particle picture for the corresponding measurement in Fig. 2(b) and their atomic orbital character. A MO illustration based on density functional theory calculations is given in the middle. (b) Experimental $2t_{1u} - 6a_{1g}$ doublet absorption spectra under the influence of strong IR fields. For each IR intensity, an offset of 2×10^{-2} OD was applied for better perspective visibility. Therefore, two exemplary ordinate axes are given on the left for the extreme cases of lowest (black) and highest (red) IR intensity. (c) Experimental and fitted R (red) and Δ (blue) dependencies on IR electric field strength. The insets show the Voigt fits for the values used for the analytical model fit.

172.27 eV, respectively [43]. Thus, we probe the electronic structure of SF_6 from the point of view of the sulfur atom [16]. The orbitals $2t_{1u}$ and $6a_{1g}$ represent the core and valence orbitals from the model in Fig. 1(a). The $6a_{1g}$ orbital [43–45] has a significant exchange interaction with the S $2p$ core orbital $2t_{1u}$. Consequently, the $2t_{1u} \rightarrow 6a_{1g}$ transition is an ideal probe for the interaction between the five remaining $2t_{1u}$ electrons and the excited LUMO electron, referred to as core-hole–excited-electron interaction [46]. In addition, a strong IR laser pulse dipole couples the $6a_{1g}$ with other unoccupied orbitals with odd symmetry, e.g., $6t_{1u}$. The manifold of dipole-coupled odd-parity orbitals represents the effective polarizing orbital ψ_p in Fig. 1(a).

The experimental implementation sketched in Fig. 1(b) employs a few-optical-cycles pulsed IR laser source at a center wavelength of 1535 nm. A pulse energy of 1 mJ is used for the experiment and focused into an XAS vacuum beam line. The SXR pulses are produced via high-order harmonic generation (HHG), resulting in a continuous spectrum up to 200 eV. By cutting the beam mode of the residual, divergent IR after HHG with a motorized aperture, the IR intensity can be controlled. Afterward, the SXR and the IR beams are refocused into a gaseous SF_6 target. Finally, the transmitted SXR beam is spectrally dispersed and measured with a CCD camera (see Supplemental Material, Sec. I [33]).

Figure 2(b) shows the experimentally determined $6a_{1g}$ doublet absorbance for different IR intensities. Using a Voigt fit model (see Supplemental Material, Sec. II [33]), one can extract the area ($A_{1/2}$ and $A_{3/2}$, respectively) and center-energy position ($E_{1/2}$ and $E_{3/2}$, respectively) of each absorption peak within the doublet. In XAS, the absorbance peak area of a resonance is proportional to the oscillator strength of the respective transition. As can be seen in Fig. 2(b), $A_{1/2}$ grows, whereas $A_{3/2}$ decreases for higher IR field strengths. Consequently, the peak area ratio $R = (A_{3/2}/A_{1/2})$ is reduced by $53 \pm 4\%$ [compare Fig. 2(c)]. Measurements of the unperturbed SXR absorption spectrum showed that SF_6 is an exemplary electron-correlation-influenced system in which Hund's multiplicity rule does not apply, as $A_{3/2}$ is smaller than $A_{1/2}$ instead of being statistically twice as large [43,44,46]. A further suppression of the j_+ peak with increasing IR field strength intuitively suggests that the effective core-hole–excited-electron exchange interaction is further increased. To test this hypothesis, one can apply the fit model from Eq. (1): By using the peak-energy position differences ($\Delta = E_{1/2} - E_{3/2}$) and areas of just the measured static absorption spectrum at lowest IR intensity and the most perturbed absorption spectrum at highest IR intensity, one can obtain the constant Hamiltonian matrix elements [47]. For this description, $\mathcal{E}'$ is to be understood as the average field the molecules experience in the experiment. This results in the fits of $R(\mathcal{E}')$ and $\Delta(\mathcal{E}')$ as red- and blue-dashed lines in Fig. 2(c), which agree very well with the experimental data, even between the two extremal values that were exclusively used for the fit shown in the insets.

Evaluating the results of the fit, we find that the exchange interaction with the core orbital is significantly larger for the polarizing orbital than for the valence orbital, $E'_x \approx 2.5 E_x$. To understand the generality of this phenomenon, one has to consider that every dipole excitation changes the parity. Thus, the orbitals involved in the SXR dipole excitation, $2t_{1u}$ and $6a_{1g}$, have opposite parities, while the additional IR excitation flips the parity again for the polarizing orbitals. The exchange matrix

elements in Eq. (1) can be calculated via (see Supplemental Material, Sec. IV [33] for a derivation)

$$E_x^{(\prime)} \propto \iint \psi_{c_-}^{\dagger}(\vec{r}_1)\psi_{o_\uparrow}^{\dagger}(\vec{r}_2)\frac{1}{|\vec{r}_1-\vec{r}_2|}\psi_{c_+}(\vec{r}_2)\psi_{o_\downarrow}(\vec{r}_1)d\vec{r}_1 d\vec{r}_2, \tag{2}$$

where ψ_o stands for the valence orbital ψ_v ($6a_{1g}$) or the polarizing orbital ψ_p, respectively. Because the product of functions with different parities is always odd and $(1/|\vec{r}_1-\vec{r}_2|)$ is always positive, spatial changes of the sign of the integrand occur. Consequently, the exchange-integral evaluation leads to a reduced value for the alternating-parity case in comparison to the equal-parity case.

In order to extract an effective core-hole–excited-electron exchange energy, the model of Eq. (1) can be reduced by introducing the mixed orbital $\psi_{m_\pm} \overset{\text{def}}{=} \alpha_\pm\psi_v + \beta_\pm\psi_p$ and replacing $|c_\pm^{-1}v^1\rangle$ with $|c_\pm^{-1}m_\pm^1\rangle$. Thus, $|c_\pm^{-1}m_\pm^1\rangle$ represent laser-dressed many-body states. The prefactors of the mixing are chosen such that the block off-diagonal $d'\mathcal{E}'$ matrix elements in Eq. (1) vanish, and that the polarizing orbital is only perturbatively populated. This transformation reduces the dominant part of the many-body Hamiltonian to a 3×3 matrix and accounts for the effect of the field $\mathcal{E}'$ on the system by introducing effective parameters,

$$H^{\text{eff}} = \begin{array}{c} \begin{matrix} |0\rangle & |c_+^{-1}m_+^1\rangle & |c_-^{-1}m_-^1\rangle \end{matrix} \\ \begin{pmatrix} 0 & d_+^{\text{eff}}\mathcal{E} & d_-^{\text{eff}}\mathcal{E} \\ d_+^{\text{eff}}\mathcal{E} & E_+^{\text{eff}} & \boldsymbol{E_x^{\text{eff}}} \\ d_-^{\text{eff}}\mathcal{E} & \boldsymbol{E_x^{\text{eff}}} & E_-^{\text{eff}} \end{pmatrix} \end{array}, \tag{3}$$

with the effective dipole moments including multiplicity factors $d_\pm^{\text{eff}}$, the energy expectation values of $|c_+^{-1}m_+^1\rangle$ and $|c_-^{-1}m_-^1\rangle$, $E_\pm^{\text{eff}}$, respectively, and the effective exchange energy E_x^{eff}. In general, the effective parameters depend on the field strength $\mathcal{E}'$. The value of E_x^{eff} can be found from Eq. (2) by replacing $\psi_{o_{\downarrow/\uparrow}}$ with $\psi_{m_\pm}$. Thus, the symmetry breaking of $6a_{1g}$ due to $6t_{1u}$ polarizing admixture, which is visualized in Fig. 3(a), leads to a larger exchange-energy value for higher IR field strengths.

Information about the effective exchange interaction can alternatively be obtained without any assumptions about microscopic quantities: By using effective parameters, $H^{\text{eff}}|_{\mathcal{E}=0}$ can be diagonalized analytically, which is conducted in the Supplemental Material, Sec. V [33] for arbitrary values of l. By making use of the fact that the effective dipole-moment ratio in Eq. (3) remains close to the multiplicity ratio, i.e., $(d_+^{\text{eff}}/d_-^{\text{eff}}) \approx (\mu_+/\mu_-)$, one can extract an equation that implicitly connects the effective exchange E_x^{eff} to the experimentally accessible area ratio R and energy splitting Δ [48]. The values displayed in Fig. 3(b) are obtained in this fashion and show an E_x^{eff} increase of up to 50% via strong IR fields in comparison to the unperturbed case.

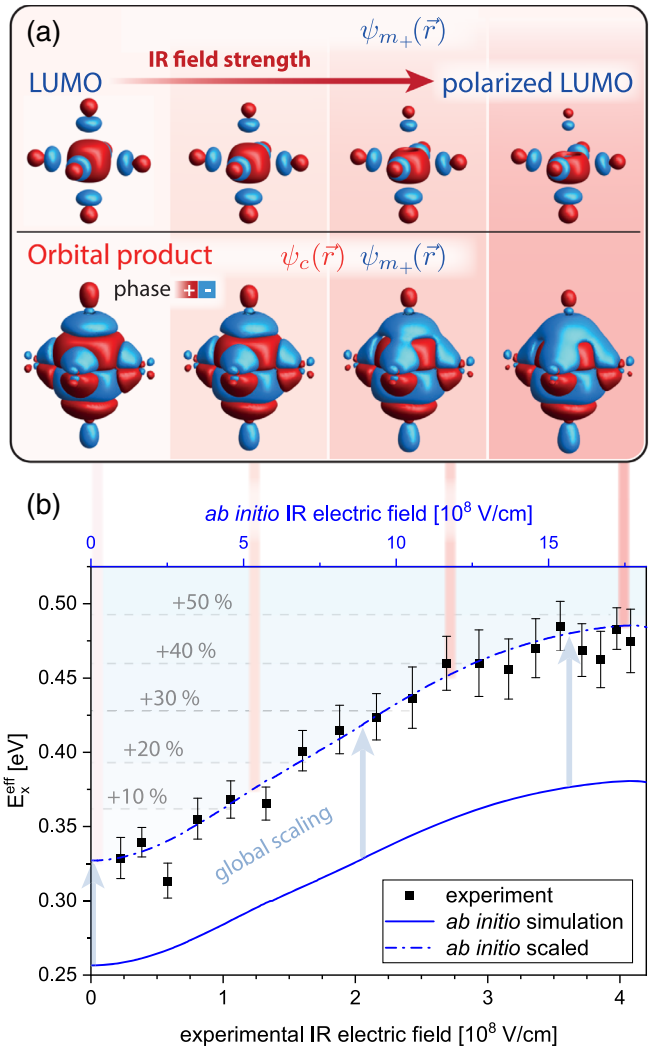

FIG. 3. Laser control of effective exchange interaction. (a) Mixed orbital ψ_{m_+} (polarized LUMO) isosurfaces for four different IR field strengths (top row) and its product with the $2t_{1u}$ core hole (bottom row), $\psi_c\psi_{m_+}$. (b) Effective exchange energy E_x^{eff} as obtained from experiment and from the *ab initio* simulation.

Our findings are supported by an *ab initio* quantum-mechanical many-body simulation in the form of a restricted active space calculation [49]. The Supplemental Material, Sec. VII [33] provides more details. The simulation result agrees qualitatively with the experimentally determined exchange energy as shown in Fig. 3(b). Quantitative agreement is shown by (i) linearly scaling the electric field strength, as well as (ii) the field-free effective exchange energy. This is necessary due to well-known shortcomings of the *ab initio* technique: Only one polarizing orbital is included in the simulation, while in reality, the IR couples to many. This leads to an underestimation of the polarizability and thus requires rescaling (i).

Furthermore, the discrepancy in the field-free case (ii) originates from underestimating the Coulomb interaction since ground-state density functional theory orbitals are also used for the excited states in the simulation.

In summary, the concept of effective electronic exchange-interaction control by strong laser fields has been introduced. By manipulating the exchange interaction of a core hole with its local excitation inside an SF_6 molecule, we experimentally implement and validate this approach. Future studies of the fundamentals of exchange-interaction control can also be carried out in atomic systems, as the only prerequisite is a spin-orbit-split core-electron transition to a very short-lived excited state. This proof-of-principle study about exchange-interaction manipulation will motivate further experiments about the details of the described mechanism, including the role of geometrical effects linked to alignment and polarization of the contributing electric fields. Furthermore, one can benefit from the generality of the presented model and replace the x-ray pulse with a visible or IR one. Hence, interactions between the HOMO and the LUMO could be modified instead of core-LUMO excitations. As the exchange interaction plays a key role in determining molecular potential-energy surfaces and chemical reactions, the presented results pave the way for using lasers as chemical agents on the fundamental electronic quantum level to selectively control molecular and material properties.

We thank C. Kaiser and his team for technical support. We acknowledge financial support by the Deutsche Forschungsgemeinschaft (DFG, German Research Foundation) under Germany's Excellence Strategy EXC2181/1-390900948 (the Heidelberg STRUCTURES Excellence Cluster) and by the European Research Council (ERC) (X-MuSiC 616783).

*patrick.rupprecht@mpi-hd.mpg.de
†christian.ott@mpi-hd.mpg.de
‡thomas.pfeifer@mpi-hd.mpg.de
§Also at Center for Quantum Dynamics, Ruprecht-Karls-Universität Heidelberg, Im Neuenheimer Feld 226, 69120 Heidelberg, Germany.

[1] W. Pauli, Über den Zusammenhang des Abschlusses der Elektronengruppen im Atom mit der Komplexstruktur der Spektren, Z. Phys. **31**, 765 (1925).
[2] A. H. Zewail, Laser femtochemistry, Science **242**, 1645 (1988).
[3] R. N. Zare, Laser control of chemical reactions, Science **279**, 1875 (1998).
[4] B. J. Sussman, D. Townsend, M. Y. Ivanov, and A. Stolow, Dynamic Stark control of photochemical processes, Science **314**, 278 (2006).
[5] T. Baumert, M. Grosser, R. Thalweiser, and G. Gerber, Femtosecond Time-Resolved Molecular Multiphoton Ionization: The Na_2 System, Phys. Rev. Lett. **67**, 3753 (1991).
[6] M. Dantus, M. J. Rosker, and A. H. Zewail, Real-time femtosecond probing of "transition states" in chemical reactions, J. Chem. Phys. **87**, 2395 (1987).
[7] A. Assion, T. Baumert, M. Bergt, T. Brixner, B. Kiefer, V. Seyfried, M. Strehle, and G. Gerber, Control of chemical reactions by feedback-optimized phase-shaped femtosecond laser pulses, Science **282**, 919 (1998).
[8] E. T. Karamatskos, S. Raabe, T. Mullins, A. Trabattoni, P. Stammer, G. Goldsztejn, R. R. Johansen, K. Długołecki, H. Stapelfeldt, M. J. Vrakking, S. Trippel, A. Rouzée, and J. Küpper, Molecular movie of ultrafast coherent rotational dynamics of OCS, Nat. Commun. **10**, 3364 (2019).
[9] J. L. Herek, W. Wohlleben, R. J. Cogdell, D. Zeidler, and M. Motzkus, Quantum control of energy flow in light harvesting, Nature (London) **417**, 533 (2002).
[10] T. Brixner, J. Stenger, H. M. Vaswani, M. Cho, R. E. Blankenship, and G. R. Fleming, Two-dimensional spectroscopy of electronic couplings in photosynthesis, Nature (London) **434**, 625 (2005).
[11] F. Siegrist, J. A. Gessner, M. Ossiander, C. Denker, Y.-P. Chang, M. C. Schröder, A. Guggenmos, Y. Cui, J. Walowski, U. Martens, J. K. Dewhurst, U. Kleineberg, M. Münzenberg, S. Sharma, and M. Schultze, Light-wave dynamic control of magnetism, Nature (London) **571**, 240 (2019).
[12] R. R. Subkhangulov, A. B. Henriques, P. H. O. Rappl, E. Abramof, T. Rasing, and A. V. Kimel, All-optical manipulation and probing of the d–f exchange interaction in EuTe, Sci. Rep. **4**, 1 (2014).
[13] D. Fausti, R. Tobey, N. Dean, S. Kaiser, A. Dienst, M. C. Hoffmann, S. Pyon, T. Takayama, H. Takagi, and A. Cavalleri, Light-induced superconductivity in a stripe-ordered cuprate, Science **331**, 189 (2011).
[14] Z.-H. Loh, M. Khalil, R. E. Correa, R. Santra, C. Buth, and S. R. Leone, Quantum State-Resolved Probing of Strong-Field-Ionized Xenon Atoms Using Femtosecond High-Order Harmonic Transient Absorption Spectroscopy, Phys. Rev. Lett. **98**, 143601 (2007).
[15] E. Goulielmakis, Z.-H. Loh, A. Wirth, R. Santra, N. Rohringer, V. S. Yakovlev, S. Zherebtsov, T. Pfeifer, A. M. Azzeer, M. F. Kling, S. R. Leone, and F. Krausz, Real-time observation of valence electron motion, Nature (London) **466**, 739 (2010).
[16] Y. Pertot, C. Schmidt, M. Matthews, A. Chauvet, M. Huppert, V. Svoboda, A. von Conta, A. Tehlar, D. Baykusheva, J.-P. Wolf, and H. J. Wörner, Time-resolved x-ray absorption spectroscopy with a water window high-harmonic source, Science **355**, 264 (2017).
[17] A. R. Attar, A. Bhattacherjee, C. D. Pemmaraju, K. Schnorr, K. D. Closser, D. Prendergast, and S. R. Leone, Femtosecond x-ray spectroscopy of an electrocyclic ring-opening reaction, Science **356**, 54 (2017).
[18] N. Saito, H. Sannohe, N. Ishii, T. Kanai, N. Kosugi, Y. Wu, A. Chew, S. Han, Z. Chang, and J. Itatani, Real-time observation of electronic, vibrational, and rotational dynamics in nitric oxide with attosecond soft x-ray pulses at 400 eV, Optica **6**, 1542 (2019).
[19] R. Geneaux, H. J. B. Marroux, A. Guggenmos, D. M. Neumark, and S. R. Leone, Transient absorption spectroscopy using high harmonic generation: A review of ultrafast

x-ray dynamics in molecules and solids, Phil. Trans. R. Soc. A **377**, 20170463 (2019).
[20] M. Rebholz, T. Ding, V. Despré, L. Aufleger, M. Hartmann, K. Meyer, V. Stooß, A. Magunia, D. Wachs, P. Birk, Y. Mi, G. D. Borisova, C. C. Castanheira, P. Rupprecht, G. Schmid *et al.*, All-XUV Pump-Probe Transient Absorption Spectroscopy of the Structural Molecular Dynamics of Di-iodomethane, Phys. Rev. X **11**, 031001 (2021).
[21] C. Ott, A. Kaldun, P. Raith, K. Meyer, M. Laux, J. Evers, C. H. Keitel, C. H. Greene, and T. Pfeifer, Lorentz meets Fano in spectral line shapes: A universal phase and its laser control, Science **340**, 716 (2013).
[22] M. Wu, S. Chen, S. Camp, K. J. Schafer, and M. B. Gaarde, Theory of strong-field attosecond transient absorption, J. Phys. B **49**, 062003 (2016).
[23] C.-T. Liao and A. Sandhu, XUV transient absorption spectroscopy: Probing laser-perturbed dipole polarization in single atom, macroscopic, and molecular regimes, Photonics **4**, 17 (2017).
[24] M. B. Gaarde, C. Buth, J. L. Tate, and K. J. Schafer, Transient absorption and reshaping of ultrafast XUV light by laser-dressed helium, Phys. Rev. A **83**, 013419 (2011).
[25] H. Wang, M. Chini, S. Chen, C.-H. Zhang, F. He, Y. Cheng, Y. Wu, U. Thumm, and Z. Chang, Attosecond Time-Resolved Autoionization of Argon, Phys. Rev. Lett. **105**, 143002 (2010).
[26] Y. Onodera and Y. Toyozawa, Excitons in alkali halides, J. Phys. Soc. Jpn. **22**, 833 (1967).
[27] B. T. Thole and G. van der Laan, Branching ratio in x-ray absorption spectroscopy, Phys. Rev. B **38**, 3158 (1988).
[28] In the following, peak area ratio and spin-orbit branching ratio are used synonymously.
[29] F. M. F. de Groot, H. Elnaggar, F. Frati, R.-P. Wang, M. U. Delgado-Jaime, M. van Veenendaal, J. Fernandez-Rodriguez, M. W. Haverkort, R. J. Green, G. van der Laan, Y. Kvashnin, A. Hariki, H. Ikeno, H. Ramanantoanina, C. Daul *et al.*, $2p$ x-ray absorption spectroscopy of 3d transition metal systems, J. Electron Spectrosc. Relat. Phenom. **249**, 147061 (2021).
[30] N. V. Vitanov, A. A. Rangelov, B. W. Shore, and K. Bergmann, Stimulated Raman adiabatic passage in physics, chemistry, and beyond, Rev. Mod. Phys. **89**, 015006 (2017).
[31] O. Smirnova, Y. Mairesse, S. Patchkovskii, N. Dudovich, D. Villeneuve, P. B. Corkum, and M. Y. Ivanov, High harmonic interferometry of multi-electron dynamics in molecules, Nature (London) **460**, 972 (2009).
[32] A. Marciniak, S. Marcantoni, F. Giusti, F. Glerean, G. Sparapassi, T. Nova, A. Cartella, S. Latini, F. Valiera, A. Rubio, J. van den Brink, F. Benatti, and D. Fausti, Vibrational coherent control of localized d–d electronic excitation, Nat. Phys. **17**, 368 (2021).
[33] See Supplemental Material at http://link.aps.org/supplemental/10.1103/PhysRevLett.128.153001 for further information on the experimental setup, the data evaluation, as well as the minimal model and *ab initio* simulation, which includes Refs. [34–40].
[34] J. R. Taylor, *Error Analysis* (University Science Books, Sausalito, California, 1997).
[35] F. M. F. de Groot and A. Kotani, *Core Level Spectroscopy of Solids* (CRC Press, Boca Raton, FL, 2008).
[36] M. W. Haverkort, M. Zwierzycki, and O. K. Andersen, Multiplet ligand-field theory using Wannier orbitals, Phys. Rev. B **85**, 165113 (2012).
[37] M. W. Haverkort *et al.*, Quanty website, http://www.quanty.org (2021).
[38] K. Koepernik and H. Eschrig, Full-potential nonorthogonal local-orbital minimum-basis band-structure scheme, Phys. Rev. B **59**, 1743 (1999).
[39] K. Koepernik *et al.*, FPLO website, https://www.fplo.de (2021).
[40] P. B. Corkum and F. Krausz, Attosecond science, Nat. Phys. **3**, 381 (2007).
[41] K. G. Wilson, The renormalization group: Critical phenomena and the Kondo problem, Rev. Mod. Phys. **47**, 773 (1975).
[42] P. A. M. Dirac, The quantum theory of the emission and absorption of radiation, Proc. R. Soc. A **114**, 243 (1927).
[43] E. Hudson, D. A. Shirley, M. Domke, G. Remmers, A. Puschmann, T. Mandel, C. Xue, and G. Kaindl, High-resolution measurements of near-edge resonances in the core-level photoionization spectra of SF_6, Phys. Rev. A **47**, 361 (1993).
[44] J. L. Dehmer, Evidence of effective potential barriers in the x-ray absorption spectra of molecules, J. Chem. Phys. **56**, 4496 (1972).
[45] Y. Sato, K. Ueda, H. Chiba, E. Shigemasa, and A. Yagishita, Auger-electron-photoion and photoion-photoion coincidence studies on ionic fragmentation of SF_6 following the S L-shell excitation, Chem. Phys. Lett. **196**, 475 (1992).
[46] M. Kadek, L. Konecny, B. Gao, M. Repisky, and K. Ruud, X-ray absorption resonances near $L_{2,3}$-edges from real-time propagation of the Dirac-Kohn-Sham density matrix, Phys. Chem. Chem. Phys. **17**, 22566 (2015).
[47] The matrix element fit values of Eq. (1) are as follows: Variable, $\mathcal{E}' = 2.25 \times 10^7$ and 4.08×10^8 V cm^{-1}; fit parameters, $E'_+ = E_+ + (2.33 \pm 0.04)$, $E'_- - E'_+ = (0.15 \pm 0.05)$, and $E'_x = (0.80 \pm 0.01)$ eV; constant parameters, $\mu_+ = \sqrt{4}$, $\mu_- = \sqrt{2}$, $\mathcal{E} = 4.08 \times 10^5$ V cm^{-1}, $d\mathcal{E} \approx 0$ eV, $d' = 6.47 \times 10^{-9}\, e$ cm, $E_+ = 173$ eV, $\Delta_{jj} = E_- - E_+ = 0.9577$ eV, and $E_x = 0.3265$ eV; for more details see Supplemental Material, Sec. VI [33].
[48] In the case of SF_6 ($l = 1$): $R = \frac{-4\sqrt{2}E_x^{\mathrm{eff}} + 3\Delta + \sqrt{\Delta^2 - 4(E_x^{\mathrm{eff}})^2}}{4\sqrt{2}E_x^{\mathrm{eff}} + 3\Delta - \sqrt{\Delta^2 - 4(E_x^{\mathrm{eff}})^2}}$. In the derivation of this formula, shown in the Supplemental Material, Sec. V [33], $\frac{d_+^{\mathrm{eff}}}{d_-^{\mathrm{eff}}} \approx \frac{\mu_+}{\mu_-}$ was used. This is justified, as even for the highest experimentally used IR field strength, $\mathcal{E}' = 4.08 \times 10^8$ V cm^{-1}, the two ratios match within 5%.
[49] R. V. Pinjari, M. G. Delcey, M. Guo, M. Odelius, and M. Lundberg, Restricted active space calculations of L-edge x-ray absorption spectra: From molecular orbitals to multiplet states, J. Chem. Phys. **141**, 124116 (2014).

Correction: A proof request to replace the first term in the third complete sentence after Eq. (3) was overlooked and has been rectified. A production processing error rendered Eqs. (1) and (3) in the HTML online version improperly and has been fixed.